2015-01-2891
Published 09/29/2015

doi:10.4271/2015-01-2891
saecomveh.saejournals.org

Bluff Body Drag Reduction Using Passive Flow Control of Jet Boat Tail

Trevor Hirst, Chuanpeng Li, Yunchao Yang, Eric Brands, and Gecheng Zha
University of Miami

ABSTRACT

This paper conducts experimental study and numerical large eddy simulation for the drag reduction effect of jet boat-tail passive flow control on bluff body models. The jet boat-tail for bluff bodies operates by surrounding a converging duct around the end of a bluff body where the base surface is located. The duct captures free stream and forms a high speed jet angled toward the center of the bluff body base surface circumferentially to have the effect of a boat tail. A rectangular prism bluff body representative of various motor vehicle shapes such as trucks, vans, SUVs is used in this study. The numerical Large Eddy Simulation shows that the jet boat-tail sucks in the forebody boundary layer due to the low base pressure and significantly thins the boundary layer. The jet interacts with the shear layer and creates large vortex structures that entrain the freestream to base flow and energize it. The base pressure with the jet boat-tail is increased and the wake velocity deficit is reduced, resulting in a significant drag reduction. The Large Eddy Simulation indicates a significant drag reduction of 15%. The baseline and jet boat-tail configuration were also tested in a wind tunnel using 3D Stereo Particle Image Velocimetry at the speed of 10m/s and 30m/s. The wind tunnel testing shows a significant wake velocity deficit reduction by using jet boat-tail passive flow control, which is consistent with the drag reduction results of the Large Eddy Simulation.

CITATION: Hirst, T., Li, C., Yang, Y., Brands, E. et al., "Bluff Body Drag Reduction Using Passive Flow Control of Jet Boat Tail," *SAE Int. J. Commer. Veh.* 8(2):2015, doi:10.4271/2015-01-2891.

1. INTRODUCTION

Aerodynamic efficiency is at the forefront of concern when designing commercial road vehicles. As such, reducing aerodynamic drag has become the focal point of many research topics. Still, however, many commercial vehicles that are employed for the transportation of people and goods experience very high amounts of drag. Many of these high drag vehicles utilize configurations similar to rectangular prisms. Such vehicles include semi-trailer trucks, vans, buses, and SUV's. These vehicles are responsible for a substantial amount of miles traveled. Single-unit and combination trucks collectively consumed over 44 million gallons of gas in the US in 2010, accounting for over 26% of all gasoline consumed by motor vehicles that year[1].

A base surface is defined as a configuration ending with an abrupt cut-off by a flat or near flat surface [2]. The region immediately following the base surface is a volume that is of very low flow pressure and momentum, caused by this abrupt cut off. These characteristics make the base region a large source of drag, known as base drag. In fact, base drag is responsible for approximately 30% of all of the aerodynamic drag of a truck [2].

It is clear that reduction of this base drag would result in a noticeable reduction in the drag of the body, increasing the efficiency of the vehicle[1,2,3]. At a time when fuel consumption restrictions have become more and more stringent, base-drag reduction technologies have never been more crucial.

A plethora of base drag technologies have been explored for a variety of applications, including: base bleed, splitter wedges, splitter plates, and boat tailing [4, 5, 6]. These technologies are known as passive flow control methods. Passive flow control methods are methods in which they do not consume energy while reducing drag [7]. While these methods can be effective in reduction of drag, they are limited in their practical applications to semi-trailer trucks and other rectangular prism vehicles. Semi-trailer trucks face traffic restrictions limiting the available space for splitter plates and boat tailing [8]. Even though boat tailing is used for heavy-duty trucks with retractable panels. It is not so convenient to be used with smaller vehicles such as family vans, SUV's, cars, etc due to impeding the loading and unloading of a vehicle. In addition, base bleed requires a hole in the center of the base surface in order to allow for the formation of the counter-rotating vortex [9]. The location of such an open hole on a vehicle truck is usually unpermitted.

A concept known as Jet Boat Tail(JBT) has been previously suggested and proven effective to reduce the drag of automobile rear view mirrors by Zha and his team[10, 11,12,13,14]. This method is effective and convenient as it does not interfere with the base surface and does not create increase of the size of the body. In the previous study of the JBT flow control device, the inlet to the JBT is opened on the body of the rear view mirror model. This allows for airflow go through the model.

The purpose of this paper is to apply the passive Jet Boat Tail flow control to bluff body models, where the JBT is installed around the end part of the body and allows no flow to go through the prism itself.

2. JET BOAT TAIL CONCEPT

A conventional general bluff body model cross sectional sketch is illustrated in Figure 1, which is observed to create vortex shedding and a large wake behind the bluff body.

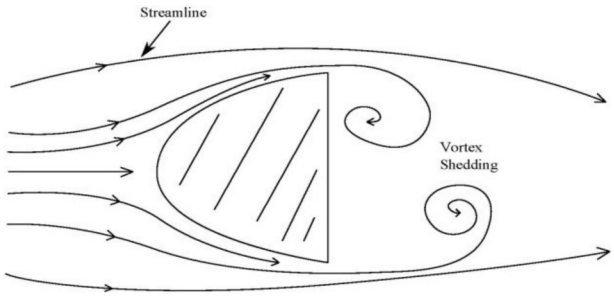

Figure 1. Vortex shedding flow structure of a general bluff body flow.

Figure 2 is a cross section sketch of the bluff body model with the passive JBT flow control implemented. The flow control concept is to utilize an open inlet at the front leading edge of the configuration, introduce airflow via a converging duct, and eject the flow through a circumferential jet from the model base surface at an angle toward the center line of the wake region.

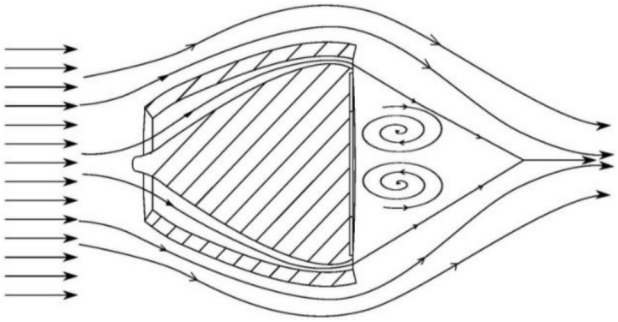

Figure 2. Expected flow structure with the jet boat tail effect influence.

2.1. Working Mechanism

The aerodynamic jet mirror working mechanism is the following [10, 11, 12, 13, 14]:

1. The jet harnesses the high kinetic energy by capturing a large amount of free stream flow with a large opened inlet in the front. It renders the jet to exit the surrounding of the mirror base with high kinetic energy and high total pressure.
2. The high energy jet creates a mixing with the main flow with large vortex structures, which entrain the main flow to the base flow and energize the base flow.
3. The angled jet toward the mirror center induces the flow to form a virtual “trailing edge” as illustrated in Figure 2, creates a more stable vortex zone behind the mirror, mitigates the vortex shedding and turbulence fluctuation, and reduces the wake size. It is well known that the aerodynamic drag is directly determined by the wake width. The smaller the wake, the smaller the drag.
4. The energized base flow and shrunk wake size increase base static pressure. The opened inlet reduces the front blockage by passing the flow and decrease the front area stagnation pressure area. These effects result in the reduced pressure drag. The reduced vortex shedding and turbulence fluctuation yields lower turbulence mixing noise that discomforts the driver and passengers.

3. THE JBT BLUFF BODY MODELS

To exhibit the benefits of the JBT passive flow control method for vehicles such as trucks, geometry models of rectangular prism with different rear end configurations are created for wind tunnel testing and large eddy simulation.

A sketch of the baseline model can be seen in Figure 3. Figure 4 shows the model with a Jet Boat Tail flow control device.

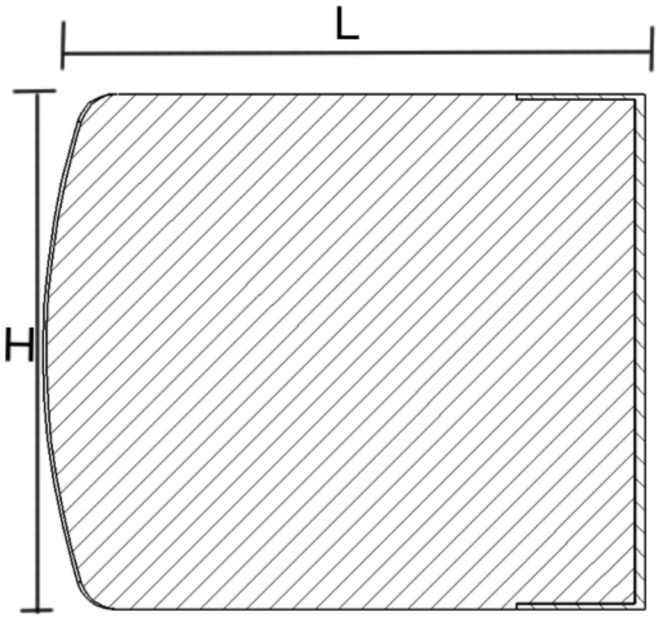

Figure 3. Cross Section of Baseline.

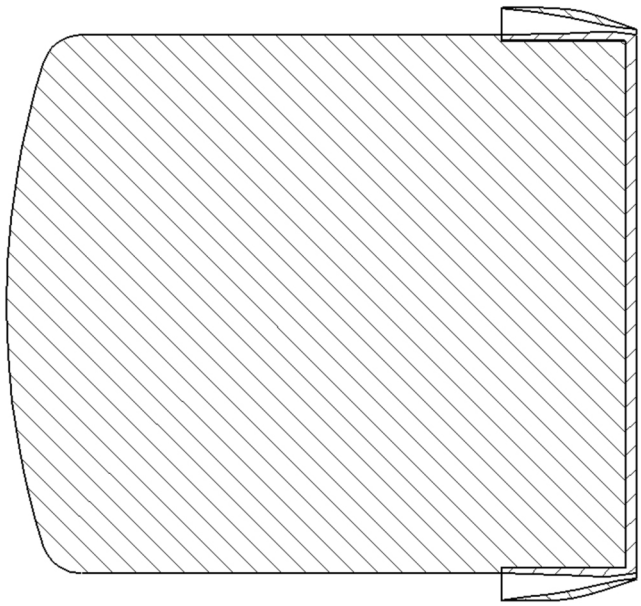

Figure 4. Cross section of model with JBT attachment.

The dimensions of the bluff body base, as seen in Figure 5, are height (H) of 200mm, a width of 150mm, and a length (L) of 230mm. The length includes a smoothly curved surface protruding upstream from the rectangular body to create the bluff characteristic.

The JBT configuration consisted of three separate pieces. These three pieces are referred to here as the bluff body base, inner shell, and outer shell. The configuration is illustrated in Figure 5.

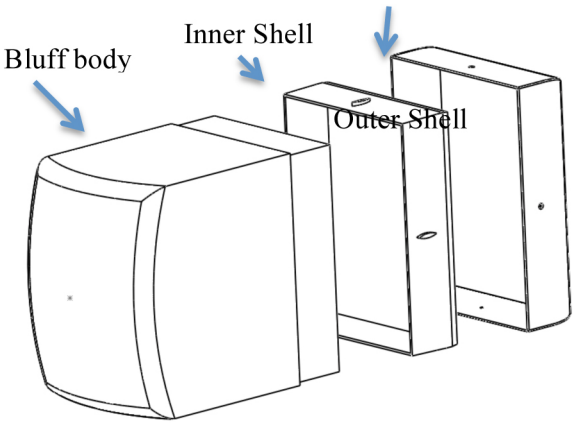

Figure 5. Exploded view of assembled model configuration.

The inlet cross sectional is uniform along all surfaces of the bluff body base, and is characterized by the gap between the inner and outer shell. The inlet height is 5% of the height of the bluff body base, which corresponds to 10mm. The outlet is similarly uniform along all surfaces, and has a height of 1%, or 2mm.

The duct length is 25%H, or 50mm. The duct profile, defined as the gap between the inner and outer shell is shown in Figure 6, converges smoothly from the inlet to the outlet. The flow exists the duct at an angle of 7° below freestream. The outer shell was defined to be as thin as possible, while still being able to maintain at high velocities, and be accurately 3D printed.

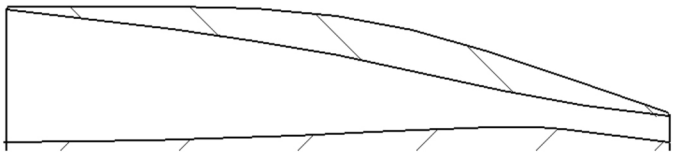

Figure 6. Profile of convergent jet section for model 10_2.

The baseline model consists of the bluff body base and an inner shell. The inner shell is created to fit smoothly and flat against the bluff body base.

4. PARTICLE IMAGE VELOCIMETRY(PIV)

All results presented here were obtained at the University of Miami Wind Tunnel Research facility. The wind tunnel used is an Open-Circuit Wind Tunnel, with test section dimensions of 24″×24″×24″ [15, 16]. The results were obtained using PIV experimentation. The model is mounted to an aluminum strut, which is attached to a load cell sting, such that the model is located in the center of the test section. Load cell data is not presented here, as the force measurements are not sensitive enough to accurately measure variations in the drag force.

A Lavision Digital Particle Velocimetry system is employed for the PIV experimentation. This system includes a Litron 135mJ Double Pulse Nd:YAG Laser and two Lavision proX2m series CCD Cameras. These Cameras are capable of recording up to 14Hz in a stereo PIV configuration. For each test, 400 samples were taken at approximately 6 Hz sample rate[17].

Table 1. PIV Instrumentation and Data Processing.

Target Flow of Measurement	
Target Flow of	2d/3C Air Flow in Wind
Uniform flow speed (m/s)	10m/s(Re=0.85x10^5), 30m/s(Re=2.56x10^5)
Tracer Particle	Di-Ethel Hexel Sebecate
Average Diameter	0.001
Light Source	Double Pulse Nd:TAG
Laser Power	800 mK
Laser Sheet Thickness	1.0mm
Time interval dt (μs)	78
Image Detection	
Camera	
Spatial Resolution	1600 x 1200 pixels
Sample Rate	~6 Hz
Pixel Size	.0074 mm x .0074 mm
Data Processing	
Pixel Unit Analysis	Stereo Cross Correlation
Correlation Area Size	64 x 64 pixels
Search Area Size	32 x 32 pixels
Integration Window	50% First Pass, 50%

An uncertainty analysis was performed in accordance with International Towing Tank Conference guidelines, resulting in a maximum uncertainty of 3.75%[18]. PIV velocity measurements of free stream were compared with Pitot tube results and found to be within 1%. The PIV plane measured for these tests was located 1/8th of the width of the model (18.75 mm) off of the center of the model as to avoid additional interference from the stabilizers.

5. RESULTS AND DISCUSSION

From the following aerodynamic drag equation

$$D = \int_{\delta} \rho u(u_{\infty} - u)dy \quad (1)$$

where δ is the width of the wake, it can be seen that a reduction in the area of the wake or a reduction in the velocity deficit would yield a reduction in drag. The numerical simulation and wind tunnel testing are hence focused on examining the wake size.

5.1. Wind Tunnel Testing

The results of the PIV testing yield velocity vectors u, v, and w, for the x, y, and z directions respectively. All of this data was collected 1/8th the width the model off of midplane as shown in Figure 7a. All results presented here are time averaged from the 400 samples collected and post processed under the conditions discussed previously given in Table 1. Fig. 7b is the JBT bluff model installed in the wind tunnel for testing.

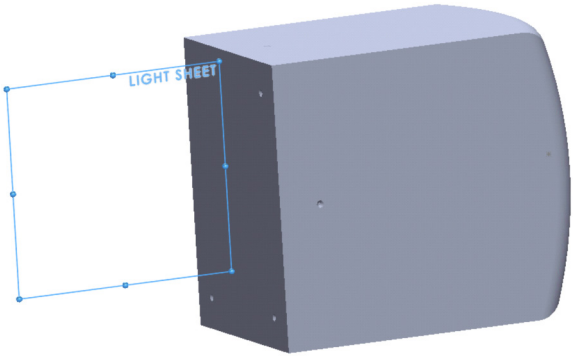

Figure 7a. Location of light Sheet on baseline model.

Figure 7b. The JBT bluff body installed in the wind tunnel for testing.

Figure 8 and Figure 9 show the contours plots of velocity magnitude V_{tot} and planar streamlines parallel to the free stream flow. The distance downstream is normalized to the length L. The velocity magnitude is normalized to the free stream velocity. The distance from the center of the model y, is normalized to the height.

It can be seen that the JBT configuration has a large impact on the recirculation zone of the wake, reducing the overall recirculation zone length significantly. This effect is slightly more pronounced in the 30 m/s data set as shown in Figure 9, compared to the 10 m/s data set. The reduction of the recirculation zone is consistent with LES results to be shown in next section.

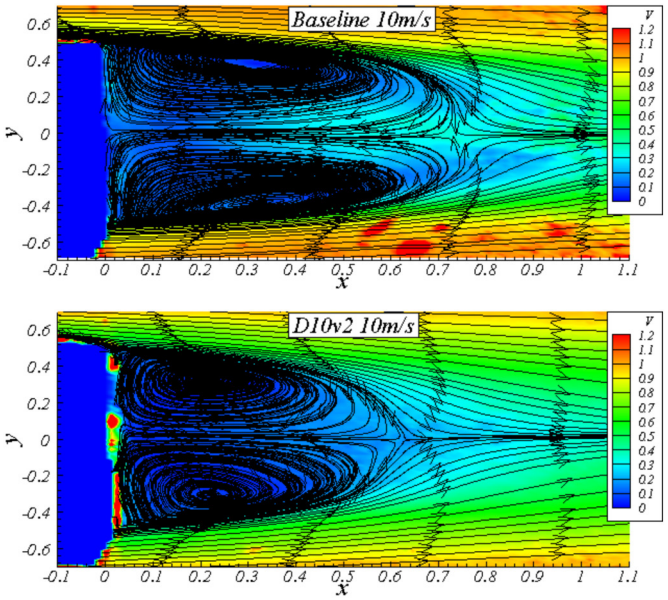

Figure 8. Average velocity contours and streamlines for baseline and JBT model at V=10 m/s.

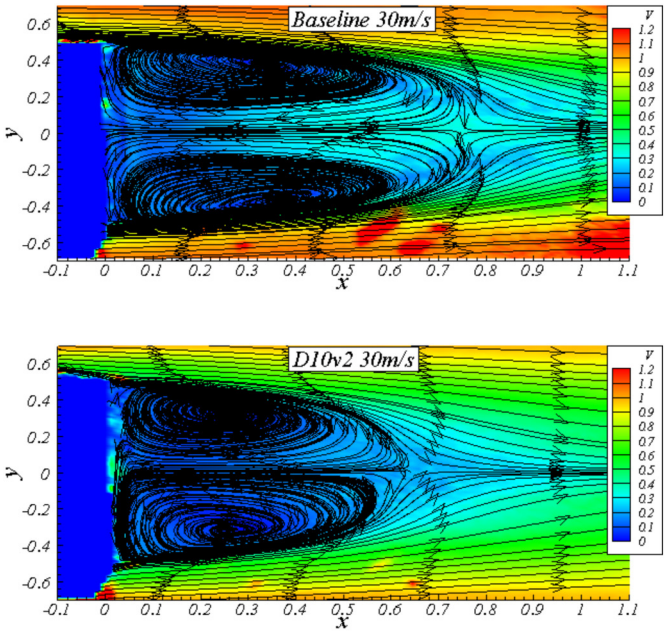

Figure 9. Average velocity contours and streamlines for baseline and JBT models for V=30m/s.

Figure 10 shows the streamwise velocity component u profile at a distance 80%H downstream. The velocity deficit of the JBT bluff body model is significantly less than the baseline model. However, the outer part of the velocity profile has more deficit due to the

increased captured area of the JBT duct. But the overall effect is a net gain of drag reduction as quantitatively shown later by the LES results.

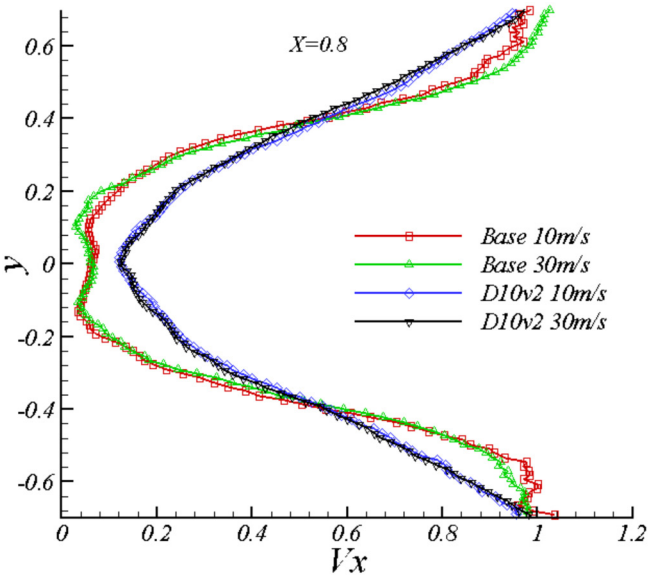

Figure 10. Average velocity profile at 80%H downstream for Baseline and JBT models.

5.2. Large Eddy Simulation

To investigate the details of the flow structures and mixing mechanisms of the JBT passive flow control for bluff body model drag reduction, a Large Eddy Simulation (LES) of the experiment models is conducted. The implicit LES methodology suggested by Shen et al. [19] is used in the LES study. The Low Diffusion E-CUSP (LDE) Scheme and the third-order finite difference WENO scheme is employed to evaluate the inviscid fluxes.[20] The dual time stepping method is used to solve the time dependent governing equations with implicit pseudo time marching scheme and unfactored Gauss-Seidel line relaxation.

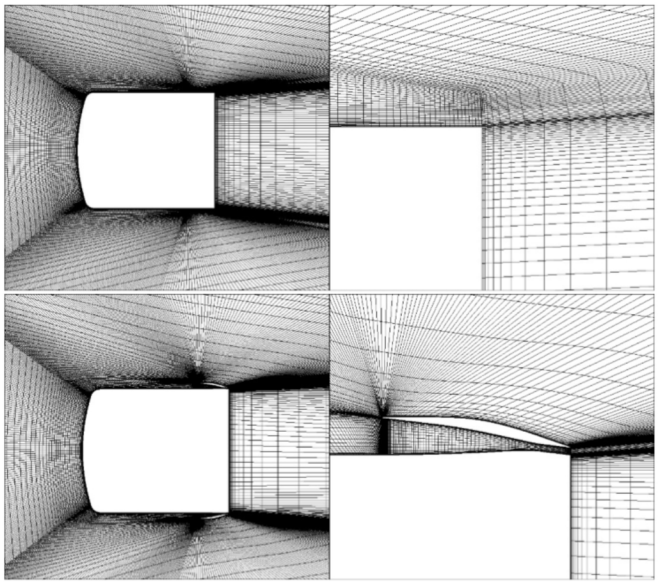

Figure 11. Cross section of mesh topology for Bluff body baseline and JBT 10_2 model (Top left: baseline mesh overview, top right: mesh at rear tip of baseline model) (Bottom left: JBT 10_2 mesh overview, bottom right: mesh inside jet of JBT 10_2 model).

The baseline model and Jet model with inlet height of 10mm and outlet height of 2mm (Jet 10_2 model) is investigated with LES. Simulations are conducted with the free stream speed of 30 m/s and Reynolds number of 2.56×10^5 based on the baseline mirror length. The non-dimensional time step used is 0.02.

5.2.1. LES Mesh Generation

The far field boundary is set at 50 times characteristic length of baseline mirror model. The no-slip boundary condition is applied on all the wall surfaces. Two multiblock structured meshes are generated for the LES calculations as shown in Figure 11. For the baseline bluff body model, a 302-blocks mesh with size of 17.76 million cells is generated with very fine mesh in the wake region. For the JBT model, a 360-blocks mesh of 25.94 million cells is generated, with refined mesh near the tunnel region and wake region. The y^+ is calculated from the normal distance of the first wall grid and is mostly less than 1, as shown in Figure 12.

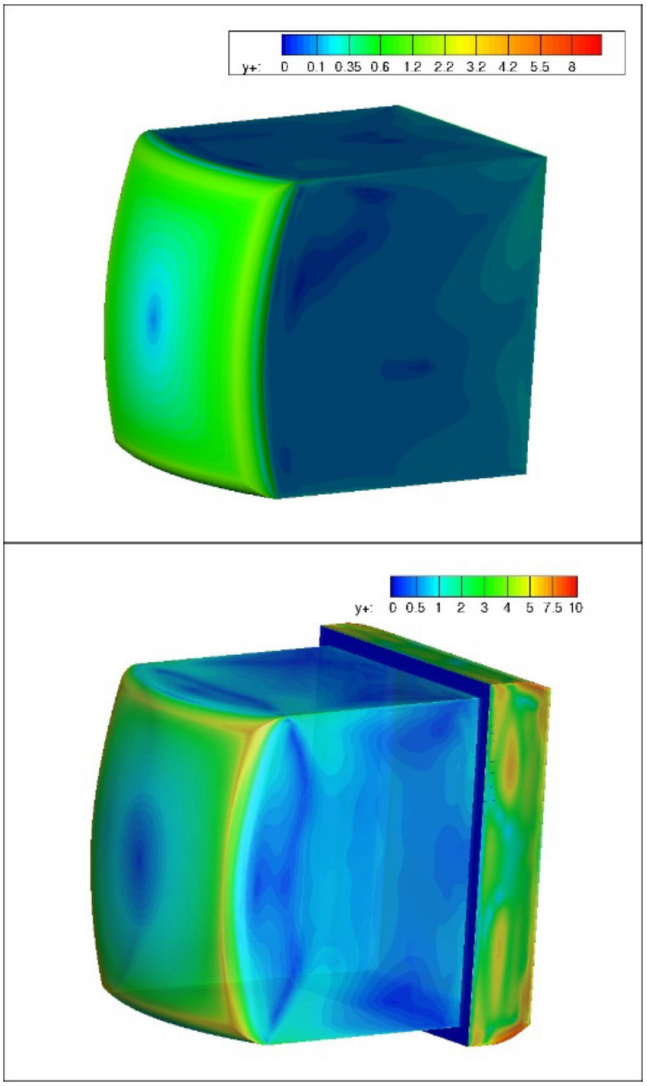

Figure 12. Calculated y^+ from normal distance of the first wall grid for baseline(left) and 10_2 model(right).

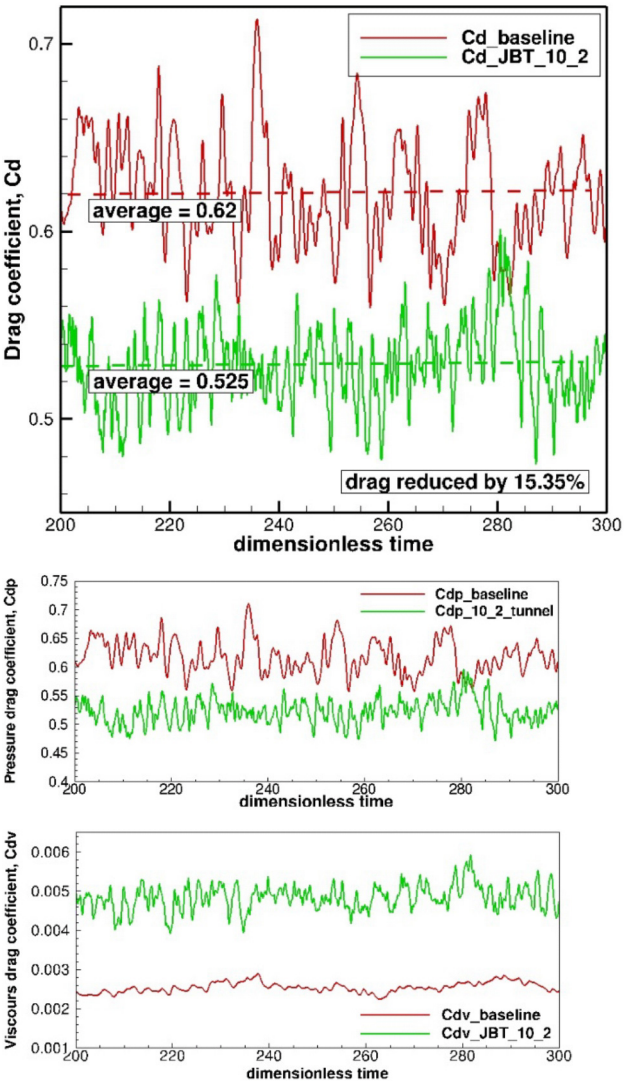

Figure 13. LES Drag coefficient history from baseline and JBT model(total drag, pressure drag and viscous drag coefficient).

5.2.2. LES Results

The Drag coefficient comparison from LES is presented from dimensionless time 200 to 300 in Figure 13. Calculated drag coefficient of baseline and JBT 10_2 model oscillate due to vortex shedding and shear layer instability. Figure 13 indicates that the drag is significantly reduced by the JBT model by 15.35%. The pressure drag coefficient and viscous drag coefficient are also given in Figure 13. It is clear that pressure drag plays a dominant role in total drag, and it is significantly reduced by introducing the JBT model. The JBT model has a larger viscous drag than the baseline model because there is more friction surface due to the for the jet duct.

The comparison of the time-averaged Mach number contours is shown in Figure 14. The speed at the exit of tunnel reaches Mach number 0.092, which is higher than the freestream Mach number of 0.088. The jet momentum is very important to enhance the entrainment and the jet interaction with the shear layer from the shell. Figure 14 indicates that the JBT duct has a strong suction effect that significantly thin the boundary layer compared with the baseline case.

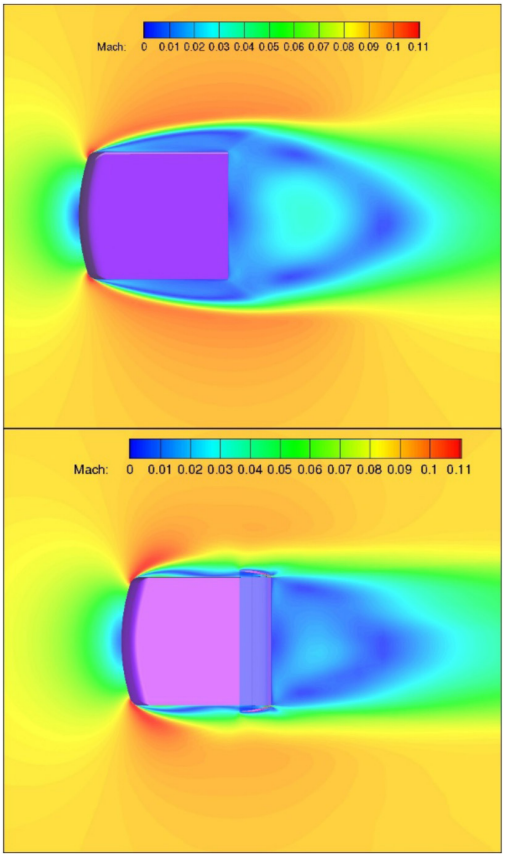

Figure 14. Time-averaged Mach number contours of baseline and JBT 10_2 model.

Figure 15 shows the time-averaged streamwise velocity component (x-component, u) contours of the baseline and JBT 10_2 model. It is very clear the shear layer area is significantly reduced by the JBT model. The streamwise velocity of the JBT model is much less negative than the baseline model and indicates a shallower wake velocity deficit.

Figure 16 is the time-averaged total pressure contours of the baseline and JBT 10_2 model. It is clearly seen that the baseline model has a much larger high total pressure loss area than the JBT 10_2 model. This indicates that the JBT model has transfer more energy from the freestream to base region via entrainment. It again shows that the JBT model has a shallower wake velocity deficit.

Figure 17 illustrates the time-averaged static pressure field of the baseline and JBT 10_2 model. The baseline model has a much larger low pressure area in the base region than the JBT model. The high base pressure of the JBT model will generates a lower drag.

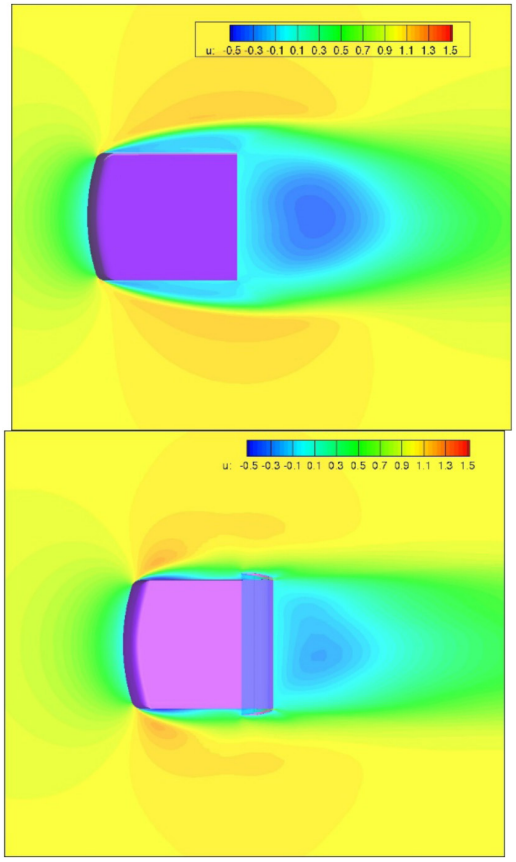

Figure 15. Time-averaged streamwise velocity component contours of baseline and JBT 10_2 model.

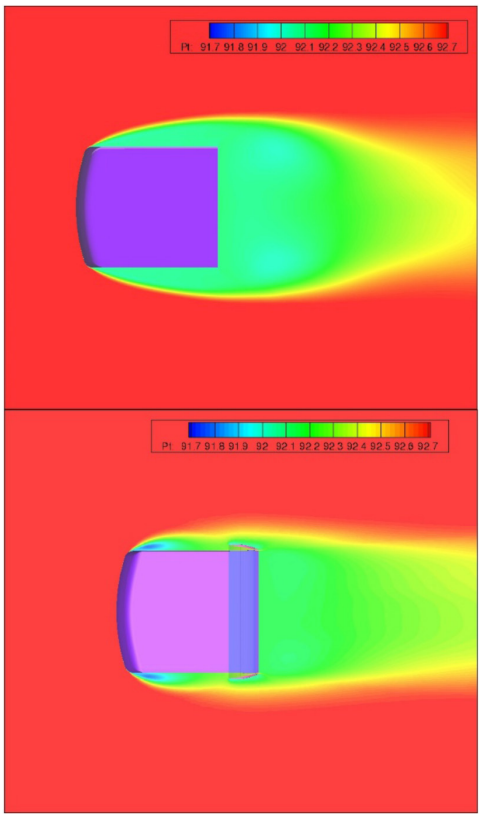

Figure 16. Time-averaged contours of total pressure component of baseline and JBT 10_2 model.

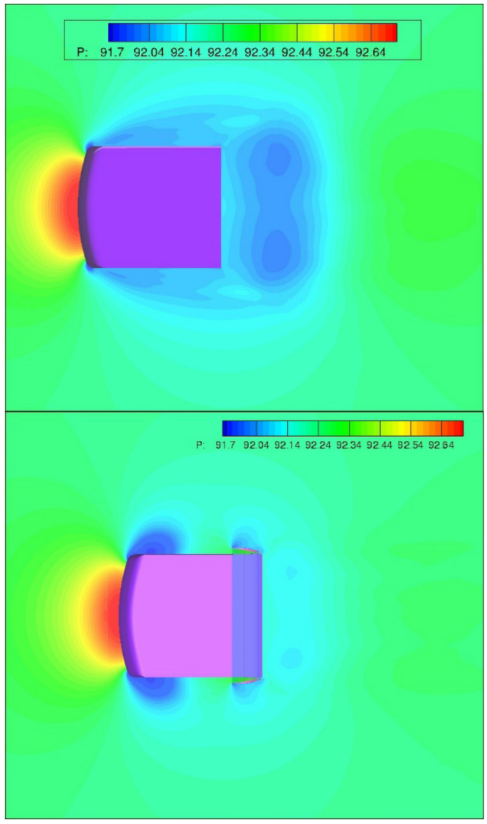

Figure 17. Time-averaged static pressure contours of baseline and JBT 10_2 model.

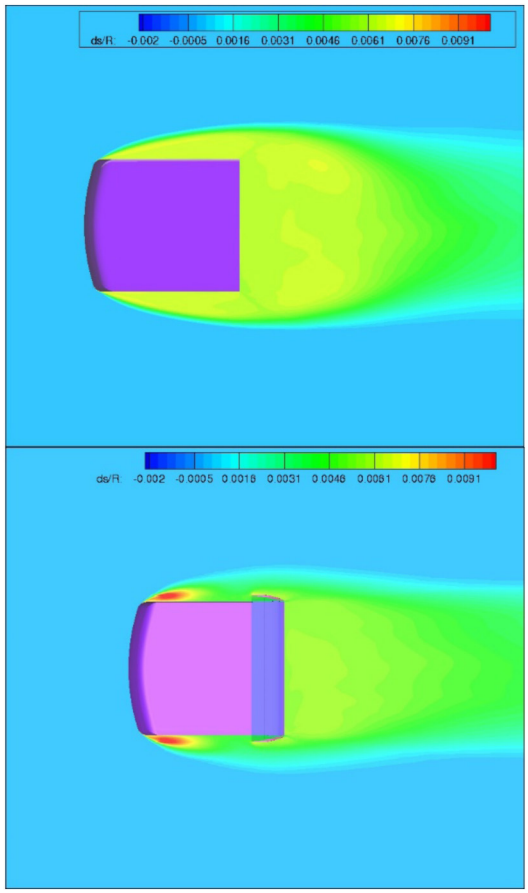

Figure 18. Time-averaged entropy contours of baseline and JBT 10_2 model

Figure 18 displays the time averaged entropy contours of baseline model and JBT 10_2 model. It is seen that the base model has a much larger high entropy area in the downstream than the JBT model. Similar to the total pressure analysis, this shows that the JBT model has a more energized base region than the baseline model to reduce drag.

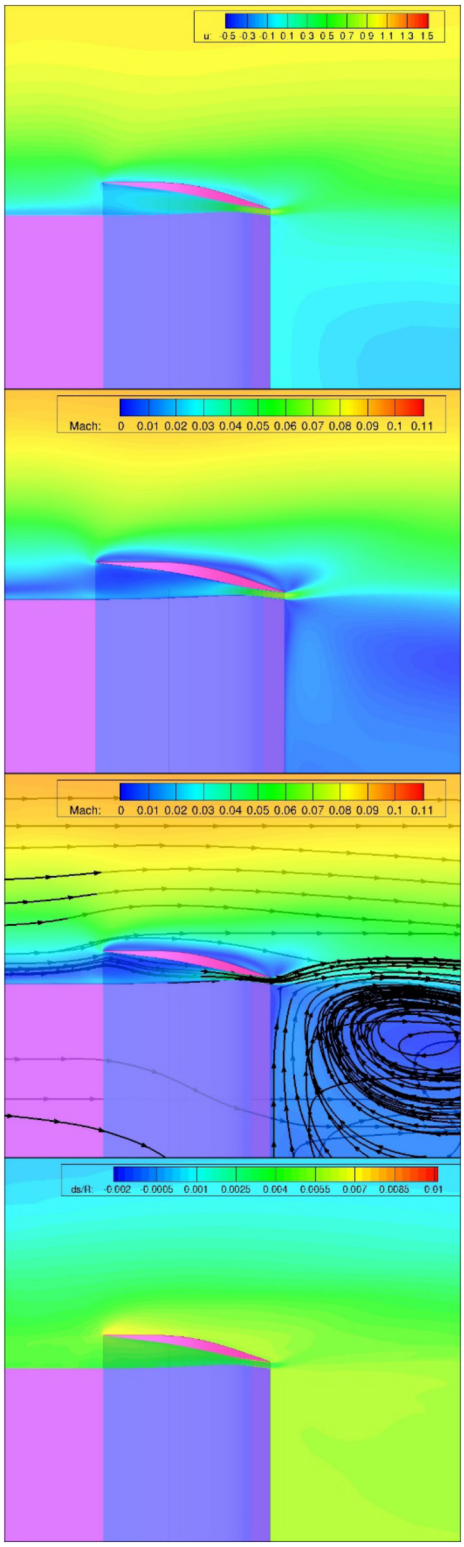

Figure 19. Time-averaged velocity u, Mach number streamline, and entropy in the jet area.

The detailed time-averaged contours of steamwise velocity, Mach number and entropy production and streamlines near the in the JBT jet area are presented in Figure 19. At the exit of jet, the maximum Mach number is about 0.09 and streamwise velocity is about the same as the free stream velocity. Entropy at the exit region of Jet is much lower than the neighbor region.

Also from the time averaged streamlines, we can see the high speed Jet entrains the free steam flow and generates a large circulation.

6. FUTURE WORK

The research is still limited in the following aspects, which will be addressed in the future work: 1) The model is not sufficiently long to reflect typical heavy duty truck configurations. 2) No yaw angle variation is studied to consider the side wind effect that is common on high way vehicle operation. 3) The recommended practice for CFD simulation and wind tunnel test given by SAE will be adopted[21,22].

7. CONCLUSIONS

This paper conducts experimental study and numerical large eddy simulation for the drag reduction effect of jet boat-tail (JBT) passive flow control on bluff body models. The JBT for bluff bodys operates by surrounding a converging duct around the end of a bluff body. The duct captures free stream and forms a high speed jet angled toward the center of the bluff body base surface circumferentially to have the effect of a boat tail. The JBT flow control device is applied to a rectangular prism bluff body model, which is representative of various motor vehicle shapes, including trucks, vans, SUVs, etc. The numerical LES shows that the JBT sucks in the forebody boundary layer due to the low base pressure and significantly thin the boundary layer. The jet interacts with the shear layer and creates large vortex structures that entrain the freestream to base flow and energize it. The base pressure with the JBT is increased and the wake velocity deficit is reduced, resulting in a significant drag reduction. The LES indicates a significant drag reduction of 15%. The baseline and JBT configuration was also tested in a wind tunnel using 3D Stereo Particle Image PIV at the speed of 10m/s and 30m/s. The wind tunnel testing shows a significant wake velocity deficit reduction by using JBT passive flow control, which is consistent with the drag reduction results of the LES. More research will be conducted to simulate more realistic heavy duty truck configurations and yaw angle effect of the incoming flow.

NOMENCLATURE

ρ - Density

L - Distance of reference length

$\mathbf{u}_{\infty}$ - Free Stream Velocity

u, v, w - Velovity components in the x, y, z Direction

$\mathbf{V}_{\mathbf{tot}}$ - Velocity magnitude, include U, V, W components

H - Height of Model

REFERENCES

1. "Highway Statistics Series." Table VM-1 - Highway Statistics 2010 - Office of Highway Policy Information (OHPI) - FHWA. Federal Highway Administration, Dec. 2012. Web. 14 Apr. 2015.
2. Hucho, W.-H., and Sovran, G., "Aerodynamics of Road Vehicles," Annual Review of Fluid Mechanics, vol. 25, pp. 485-537, 1993.
3. Krajnovic, S., and Davidson L., "Numerical Study of the Flow Around a Bus-Shaped Body," Journal of Fluids Engineering, vol. 125, pp. 500-509, 2003.
4. (Storms 2006)Storms, B. L., and Satran, D. R., and Heineck, J. T., and Walker, M., A Summary of the Experimental Results for aGeneric Tractor-Trailer in the Ames Research Center 7- by 10-Foot and 12-Foot Wind Tunnels. NASA/ TM2006-213489, 2006.
5. Maull, D. J., and Hoole B. J., The effect of boat-tailing on the flow around a two-dimensional blunt-basedaerofoil at zero incidence, J. Royal Aero. Soc., vol. 71, pp. 854858, 1967.
6. McCallen, R., DOEs Effort to reduce truck aerodynamic drag through joint experiments and computations. Presentation at the DOE Heavy Vehicle Systems Optimization Merit Review and Peer Evaluation, Argonne National Laboratory, April 18-20, 2006.
7. Tanner, M., Reduction of Base Drag, Prog. Aerospace Sci., vol. 16, No. 4, pp. 369384, 1975.
8. McCallen, R., DOEs Effort to reduce truck aerodynamic drag through joint experiments and computations. Presentation at the DOE Heavy Vehicle Systems Optimization Merit Review and Peer Evaluation, Argonne National Laboratory, April 18-20, 2006.
9. Berman, P. W., Investigation into the effect of base bleed on the flow behind a two-dimensional model with a blunt trailing edge. AGARD CP-4, Part 2, pp. 485-507, 1966.
10. Zha, G.-C., "LOW DRAG LOW NOISE DEVICES USING JET FLOW CONTROL," *Utility patent application filed to USPTO, 14/180,406, 02/14/2014*, 2014.
11. Zha, G.-C., "LOW DRAG LOW NOISE DEVICES USING JET FLOW CONTROL," *Provisional patent application filed to USPTO, 61/976,204, 04/07/2014*, 2014.
12. Zha, G.-C., "LOW DRAG LOW NOISE DEVICES USING JET FLOW CONTROL," *Provisional patent application filed to USPTO, 62/065,071, 10/17/2014*, 2014.
13. Bartow, W., Moreyra, A., Hirst, T., Woyczynski, G. et al., "Experimental Investigations of Vehicle Base Drag Reduction Using Passive Jet Boat-Tail Flow Control," SAE Technical Paper 2014-01-2448, 2014, doi:10.4271/2014-01-2448.
14. Wang, J., Bartow, W., Moreyra, A., Woyczynski, G. et al., "Low Drag Automotive Mirrors Using Passive Jet Flow Control," *SAE Int. J. Passeng. Cars - Mech. Syst.* 7(2):538-549, 2014, doi:10.4271/2014-01-0584.
15. Engineering Laboratory Design, INC. "Model 406," http://www.eldinc.com/pages/Model406/, 2009
16. Kirk, D., Experimental and Numerical Investigations of a High Performance Co-Flow Jet Airfoil, Masters Thesis, Mechanical Engineering Department, University of Miami, Coral Gables, 2009.
17. Lasers Litron, "Lasers for PIV Applications" http://www.litronlasers.com/pdf%20files/LitronPIVProducts0109_1.pdf
18. International Towing Tank Conference Recommended Procedures and Guidelines, Uncertainty Analysis Particle Imaging Velocimetry, Sept. 2008.
19. Shen, Y.-Q., and Zha, G.-C., and Chen, X.-Y., "High Order Conservative Differencing for Viscous Terms and the Application to Vortex-Induced Vibration Flows,", Journal of Computational Physics, vol. 228(2), pp. 8283-8300, 2009.
20. Shen, Y.-Q., and Zha, G.-C., and Wang, B.-Y., "Improvement of Stability and Accuracy of Implicit WENO Scheme,", AIAA Journal, vol. 47, No. 2, pp. 331-344, 2009.
21. SAE International Surface Vehicle Recommended Practice, "Guidelines for Aerodynamic Assessment of Medium and Heavy Commercial Ground Vehicles Using Computational Fluid Dynamics," SAE Standard J2966, Issued Sept. 2013.
22. SAE International Surface Vehicle Recommended Practice, "SAE Wind Tunnel Test Procedure for Trucks and Buses," SAE Standard J1252, Rev. July 2012.